HOKKAIDO UNIVERSITY

Title	Wintertime extratropical cyclone frequency around Japan
Author(s)	Inatsu, Masaru; Terakura, Kazutaka
Citation	Climate Dynamics, 38(11-12), 2307-2317 https://doi.org/10.1007/s00382-011-1152-8
Issue Date	2012-06
Doc URL	http://hdl.handle.net/2115/52801
Rights	The original publication is available at www.springerlink.com
Type	article (author version)
File Information	CD38-11-12_2307-2317.pdf

Instructions for use

Hokkaido University Collection of Scholarly and Academic Papers : HUSCAP

Wintertime Extratropical Cyclone Frequency around Japan.

Masaru Inatsu and Kazutaka Terakura

Graduate School of Science, Hokkaido University, Japan
Tel: +81-11-706-3549
Fax: +81-11-706-3549
E-mail: inaz@mail.sci.hokudai.ac.jp
URL: http://www.sci.hokudai.ac.jp/~inaz/index-e.htm

Abstract

Data analysis and regional atmospheric model (RAM) experiments revealed key factors in the control of wintertime cyclone passage routes from Northeast Asia to the western North Pacific. The cyclone routes were independent of the global flow pattern in the interannual variability, while cyclone growth closely agreed with linear baroclinic theory. The RAM experiments with a different lateral boundary condition composed of a combination of monthly mean and transient components also showed that the upstream eddies are important for the track route, but the background states are not. Additionally, the RAM experiments showed that the mean flow controlled the growth rate of cyclones.

Keywords: Extratropical Cyclones, Cyclone Tracking, Regional Atmospheric Model.

1. Introduction

Storm tracks are the zones where extratropical cyclones are generated, developed and matured, and are located in the North Pacific and North Atlantic, where a strong westerly wind blows in the troposphere (Blackmon 1976; Wallace et al. 1988). Trenberth (1991) discovered storm tracks stretching from the Southern Atlantic to the mid-latitude Indian Ocean. Storm track activity is estimated as the sum of intensity of an individual eddy, which is equal to the average storm intensity multiplied by the average storm frequency. Storm activity has traditionally been estimated by using Eulerian measures such as geopotential variance, meridional heat transport, and eddy kinetic energy. Traditional Eulerian estimates of storm activity cannot properly separate intensity from frequency, but modern automated Lagrangian tracking techniques are able to evaluate them separately if various semi-objective parameters are correctly tuned (Hoskins and Hodges 2002, 2005; Murray and Simmonds 1991; Sinclair 1994). Recently, a neighbor enclosed area tracking (NEAT) algorithm developed by Inatsu (2009) evaluated the likely locations of merger and splitting events[1] for extratropical cyclones. All methods suggest that extratropical cyclones tend to develop, sometimes very rapidly, upstream of the storm track centers of the central North Pacific, the central North Atlantic, and the Indian Ocean. Indeed, many rapidly

[1] A cyclone is often distorted in its mature stage and a filament-like warm front can be separated from the main body of the cyclone. Inatsu (2009) identified this kind of separation as a split.

developing cyclones, known as bomb cyclones in Japanese synoptic weather charts (Sanders and Gyakum 1980; Yoshida and Asuma 2004; Yoshiike and Kawamura 2009), are found in these locations and on the east coast of North America, especially in the late autumn and early spring. The stages of cyclones development can be explained by linear baroclinic theory; infinitesimally small eddies develop exponentially under strong vertical wind shear (Charney 1947; Eady 1949), while the mature stage of cyclones is thought to play a significant role in their interaction with the time mean flow through barotropic energy conversion (Hoskins et al. 1983; James 1987). Assuming that the Eurasian Continent destroys synoptic-scale cyclones and that the eddies are too small to interact with the time mean flow downstream of East Asia, the cyclone tracks should follow the linear baroclinic theory in the western North Pacific and contribute to the nonlinear interaction with the time mean flow in the eastern North Pacific. Because the transient eddies can pass over the Rockies and they flow with finite-amplitude disturbances in the western North Atlantic, nonlinear interaction between time mean flow and eddies can be found anywhere in the North Atlantic.

Eulerian predictions of storm tracks explain the wintertime storm activity in the North Pacific in terms of its relationship with the time mean state (Wallace et al. 1988). In the cold season, Japan is located between the Siberian high in the west and the Aleutian low in the east. This state holds in midwinter and is often found in early and late winter, anti-correlated with seasonal variations in the storm track activity in the western North Pacific (Nakamura 1992). Moreover, Nakamura et al. (2002) suggested that the intensity of storm activity is weak during winters with a strong Aleutian low pressure, and strong when the Aleutian

low pressure is weak. This seasonal and interannual variability of storm activity has been comprehensively studied, and is well understood (Nakamura et al. 2004).

However, storm track frequency is not yet well understood. Hoskins and Hodges (2002) have constructed a global map of cyclone frequency by using their sophisticated tracking algorithm. In East Asia, two preferred routes toward the western North Pacific were observed (Adachi and Kimura 2007), and Takayabu (1991) and Inatsu (2009) discovered two preferred routes that merge to the east of Japan. The semi-subjective weather chart analysis performed by Kusaka and Kitahata (2009) also supports the analysis finding that there are two preferred routes of cyclone passage over Japan. This study showed one route through Northeast China, the Sea of Japan, and the ocean to the northeast of Japan, and a second route through Taiwan, the southern coast of Japan, and the ocean to the southeast of Japan. Cyclones following the first route are referred to as Sea of Japan cyclones and cyclones following the second route are called Nangan cyclones. Although these routes have been recognized by many Japanese synopticians (Takano 2002), the interannual variability of the route has not yet been documented with an objective statistical analysis.

The purpose of this study is to investigate whether or not the cyclone frequency depends upon the time mean flow in the area where the cyclone develops. There are two types of eddy that can develop into cyclones. The first type is a spontaneously generated eddy with small amplitude that can rapidly develop under the vertical wind shear. This is classic linear baroclinic eddy development, which has been thoroughly studied using lifecycle experiments with a numerical model (*e.g.* Thorncroft et al. 1993). The second type of eddy has finite amplitude and enters the focusing area before being advected toward the

western North Pacific while it slowly grows. This type of eddy is not well documented or understood. We will assess which types of eddies are more important for preferred cyclone routes in East Asia, using two methods. The dominant statistical modes of the interannual variability of the cyclone routes will be documented using a Lagrangian tracking algorithm. The coherent structure, if any, between planetary-scale flow and local cyclone routes may indicate the importance of the background state. We will also perform regional atmospheric model (RAM) experiments to directly solve the problem; a new method is used in this paper to evaluate the importance of upstream eddies using RAM experiments. This allows us to construct a variety of physically consistent upstream eddies in a particular region in order to investigate the effect of upstream eddies on the preferred cyclone route and whether the route is controlled by the linear baroclinic theory. The paper is organized as follows: Section 2 contains data and model experiments and the tracking method, Section 3 details the data analysis, Section 4 contains numerical experiments with a new approach to boundary conditions (BCs), and Section 5 is the discussion and conclusion.

2. Methodology

2.1. Reanalysis Data

The data used in Section 3 is the Japanese Reanalysis Data, JRA25/JCDAS, from 1979 to 2008 (Onogi et al. 2007). The data was archived at 6 hourly intervals on a 1.25°×1.25° horizontal grid. The meridional wind was set

at 850 hPa, the zonal wind at 300 hPa, and the geopotential height at 500 hPa in the Northern Hemisphere for the winter months of December, January, and February (DJF) for the data analysis. A band-pass filter with a cutoff period of 2 and 8 days was taken for the 850 hPa meridional wind for the preprocessing of the tracking. The JRA25/JCDAS data were also used as initial and boundary conditions in the model experiments in Section 4.

2.2. Regional Atmospheric Model and Experiment Design

The RAM used in Section 4 is the Japan Meteorological Agency (JMA)/Meteorological Research Institute (MRI) nonhydrostatic model (NHM), which calculates the atmosphere in a limited domain. The model has a horizontal mesh size of 50 km, 38 vertical levels and uses terrain-following coordinates. The prognostic variables of the RAM are the three-dimensional wind vectors, the potential temperature, and the densities of dry air, water vapor, cloud water, cloud ice, snow, and graupel. The RAM also has state of the art physical packages such as cloud microphysics parameterization, radiative transfer, turbulent mixing, boundary layer processes, and surface flux estimations. The Kain–Fritsch convective parameterization scheme (Kain and Fritsch 1993), is widely used for NHMs with mesh size greater than 10 km, which corrects the amount of precipitation. This version of the JMA/MRI NHM has previously been published by Saito et al. (2006).

The RAM experiments were performed on the nested area from East Asia to the western North Pacific, approximately covering the area 100°E–180° longitude and 15°N–55°N latitude. The western boundary of the model domain is

the contact line from the effect of the upstream eddies to the cyclone passage route around Japan. The entrance of the cyclone development area under the westerly jet core is 100°E longitude, while the center of the storm track activity and the area where many cyclones reach their mature stage is at 180° longitude. Because the Nangan cyclone passage route starts around Taiwan at 22°N, the southern boundary was set far enough away from the cyclone generation area. The RAM was integrated from November 15 to March 9 of the following year in all the wintertime simulation experiments.

The new method used in the experiments is the creation of many semi-artificial lateral BCs that are not entirely physically consistent with the reanalysis dataset. The 30 day mean ($\langle \bullet \rangle$) is divided by its deviation ($\bullet'$) for variables used in the RAM, such as zonal and meridional winds, temperature, geopotential height, and specific humidity, and is written as follows:

$$Q_{aa} = \langle Q_a \rangle + Q'_a, \quad (1)$$

for any variable of Q throughout the integrating period, where the subscript a denotes a corresponding DJF. The arbitrary combinations of the mean and its deviation are such that

$$Q_{ab} = \langle Q_a \rangle + Q'_b, \quad (2)$$

where subscript a is not generally equal to subscript b. The JRA25/JCDAS reanalysis dataset including 29 DJFs, was used so that a maximum of 29×29 semi artificial BCs could be created for a RAM experiment. The RAM experiments were performed for 12 BCs using 4 DJFs: 1989/90, 2007/08, 1987/88, and 1983/84 (Table 1).

2.3 Cyclone Tracking Methods

The NEAT algorithm tracking method is used in this study (Inatsu 2009). The traditional point-to-point tracking method is based on finding local minimum points and then connecting adjacent feature points temporally with semi-objective parameters and with plural variables, such as sea-level pressure and relative vorticity. However, the new area-to-area tracking method is based on tracking tempo-spatially neighboring areas in which the band-pass-filtered meridional wind at 850 hPa (Vh850) is larger than 10 m s^{-1}, when they overlap the adjacent time frame. The track density, defined as the line density along cyclone passages, is a widely used measure of the number of tracks. However, if the track density were defined without any weighting for the track line length, it would overemphasize shorter line tracks. We therefore define the unit for the line length weighted track density as L^{-1} T^{-1}, where L is the average track line length and T is the time period.

3. Data analysis

To begin with, the climatological storm activity in the data analysis is described. Figure 1a shows the DJF mean variance of Vh850, which is a conventional measure of lower tropospheric storm activity around Japan. This measure, which includes information on the frequency and intensity of cyclones and anticyclones, indicates that the Pacific storm track starts at the focusing

region. The regional maxima of the scattering variance along the Sea of Japan and Nangan routes occur at the Liaodong Peninsula, the Far East of Russia, and the southern coast of Japan. Another measure of track density (Fig. 1b), the cyclone frequency, shows a similar horizontal distribution but highlights smaller features. The large track density that extends toward the east of Japan is concentrated in the center of the track lines compared with the variance of the meridional wind. Moreover, a high-density track line is observed from Mongolia to northern Japan, which is the same as the Sea of Japan route mentioned in the introduction. While the track density indicates the Nangan route, it reaches a regional minimum in western Japan. Since the track density captures the small scale features of the track lines rather than the variance of Vh850, the track density was used as the measure for cyclone frequency.

Figure 2 shows the statistics for the primary mode of interannual variability in the DJF cyclone tracks, using an empirical orthogonal function (EOF) analysis. The spatial pattern (Fig. 2a) shows a north-south seesaw distribution of tracks, which changes between greater numbers of Nangan cyclones and Sea of Japan cyclones. The mode also involves a larger modulation in the Sea of Japan cyclones. The first EOF mode contributes 29.3% to the total variance, while the second mode contributes 12.4% (not shown); Figure 2b shows the normalized time series of the first mode. Although the first EOF mode shows a trend of 0.02 yr^{-1}, it is not statistically significant, and may be related to the recent increase in Nangan cyclones, which is possibly related to the global warming signal in the Pacific storm track (Inatsu and Kimoto 2005; Nishii et al. 2009; Yin 2005). The largest negative DJFs are in 1989/90, 1987/88, 1986/87, and 1984/85, while the largest positive DJFs are in 2007/08, 1983/84, 2002/03, and

1994/95. Four winters for the positive or negative DJFs are more than one standard deviation of the first principal component (PC). These positive and negative DJFs are hereafter called the Nangan positive and Nangan negative DJFs, respectively. The composite maps of the track density for the Nangan positive and the Nangan negative DJFs (Fig. 3) show a clear difference in the storm passage routes. In the Nangan positive DJFs there are more than 6 tracks for each DJF along the south coast of Japan (Fig. 3a), but no significant signals on the Sea of Japan route. In contrast, in the Nangan negative DJFs (Fig. 3b), there are more than 10 tracks for each DJF from Mongolia to Northern Japan with no significant signals on the Nangan route.

The relationship between the preferred cyclone routes and the global anomaly pattern was then investigated in order to clarify whether the preferred routes around Japan are controlled by the global background state, particularly the jet stream intensity. The composite maps of the 300 hPa zonal wind and the 500 hPa geopotential height (Fig. 4a, b) show little difference between the Nangan positive and negative DJFs. However, the regression of the global geopotential height onto the first EOF mode of the cyclone tracking variability (Fig. 4c) shows few signals with a statistical significant level of 5%, except for a low pressure anomaly in the upstream of the focusing area. This anomaly is related to a slight northward shift of the upper tropospheric jet, when the 300 hPa zonal wind is regressed onto the first mode (Fig. 4d). The composite and regression analyses in Fig. 4 indicate that the preferred passages of storms around Japan are almost independent of the global pattern, which is consistent with the application of linear baroclinic theory to the growth of transient eddies, but not always to cyclone routes.

4. Experimental Results

4.1 Ensemble means

Following the data analysis in Section 3, we now focus on two Nangan positive DJFs of 2007/08 and 1983/84 and two Nangan negative DJFs of 1989/90 and 1987/88 (See the data analysis in Section 3 or Fig. 2b for the selection of DJFs.). The quotient of the time mean and transient components in Eq. (1) in Section 2.2 was taken for all the variables necessary for the RAM BCs. The time mean data for the 4 DJFs are $\langle Q_{89/90} \rangle$, $\langle Q_{87/88} \rangle$, $\langle Q_{07/08} \rangle$, and $\langle Q_{83/84} \rangle$, and the transient eddy data for the 4 DJFs are $Q'_{89/90}$, $Q'_{87/88}$, $Q'_{07/08}$, and $Q'_{83/84}$. There are 16 possible combinations, although 12 experiments were performed with different BCs. The nomenclature is the combination of a prefix denoting the mean component and a suffix denoting the transient component of the BCs. P, p, N, and n refer to the DJFs of 2007/08, 1983/84, 1989/90, and 1987/88, respectively (Table 1). For example, PN refers to an experiment with a BC of the 2007/08 DJF mean with a transient component of the 1989/90 DJF.

There are two ways to effectively make an ensemble mean. The first way uses a single sign of the mean or transient component in the combinations to make an ensemble mean of PP, PN, Pp, and Pn; NP, NN, Np, and Nn; PP, NP, pP, and nP; and PN, NN, pN, and nN. These are referred to as the P*-, N*-, *P-, and *N-ensemble means. The second way uses combinations of signs to make the ensemble mean of PP, Pp, and pP; PN, pN, and Pn; NP, Np, and nP; and NN, Nn,

and nN. These are called the PP-, PN-, NP-, and NN-ensemble means. Both methods may reveal the importance of the background state or a transient eddy entering the nested domain.

Figure 5 shows the P*, N*, *P, and *N-ensemble means of the track density using the simulated results. The *P-ensemble mean (Fig. 5c) strengthens the Nangan routes, while the *N-ensemble mean (Fig. 5d) shows a two-track density maxima on the Continent and in the east of Japan. The P*- and N*-ensemble means (Fig. 5a, b) show a separation of the track density maxima in the Continent and the east of Japan; they give fewer tracks than the *N-ensemble means. The results suggest that the route of the storms does not depend on whether the mean flow component of the BCs was a positive or a negative Nangan DJF, but that it does depend on the transient component of the BCs.

Figure 6 shows the PP-, PN-, NP-, and NN-ensemble means of the track density. The PP- and NN-ensemble means should be regarded as a realistic simulation of the Nangan positive and negative DJFs, respectively. The RAM can simulate the features of the cyclone route, showing the Nangan route for the positive DJFs (Fig. 6a) and the Sea of Japan route for the negative DJFs (Fig. 6d), with the model overwhelming the local track density minimum in Western Japan. The comparison between the PN- and NP-ensemble means shows that, while the combination of the mean positive and transient negative case leads to the Sea of Japan route (Fig. 6b), the combination of the mean negative and the transient positive results in the Nangan route (Fig. 6c). These ensemble means strongly support the idea that the cyclone routes around Japan are controlled by the transient eddies that approach the focusing region, and is independent of the basic state.

Figure 7 shows the average growth rate of the tracked cyclones, which was estimated by the increase in the rate of the enclosed areas when the NEAT algorithm was applied (*cf.* Inatsu 2009). This measure, which only applies to the growth of the cyclone, shows that, although the average growth rate is less than 1 day^{-1} around Japan under the basic state of the Nangan negative DJFs (Fig. 7c), it is around 2 day^{-1} from East Asia to Japan under the basic state of the Nangan positive DJFs (Fig. 7a, b). This result is the same whether the transient component is a negative or a positive Nangan DJF. This is consistent with previous studies (Inatsu et al. 2003; Xie et al. 2002), and indicates a close relationship between the growth rate of the cyclone intensity and the background state, as predicted by linear baroclinic theory.

4.2 Sensitivity Tests

In order to check how robust the results of RAM experiments were, two typical experiments for PN and NP were used (Fig. 8), both of which are a combination of the mean state and transient eddy components with opposite signs. Although the track density statistics are unstable unless an ensemble mean is taken, the PN and NP experiments give typical structures which highlight the Sea of Japan or Nangan cyclones as their respective ensemble means. These two experiments are therefore used as a reference of some experiments for a sensitivity test.

The standard period of 30 days was used for calculating the quotient of the mean and transient components. Typical high-frequency eddies, such as extratropical cyclones, have a period of 2-8 days, therefore the boundary of mean

and transient components were changed from 30 days to 10 days. For the 110°E-150°E domain and the 20°N-60°N domain in the 1989/90 DJF, the quotient for 10-30 day Z500 fluctuation is the same as that for the > 30 day fluctuation. Figure 9 shows the track density in the PN and NP experiments with the standard period changed to 10 days. No significant differences were observed compared with the PN and NP experiments with the standard period, although the PN experiment showed fewer tracks in the northeast of Japan. The result indicates that the division period does not greatly affect the result.

The transient eddies from the upstream were divided by those from the bottom surface, and the resulting values are given as the RAM BCs[2]. If the transient eddy component from the western boundary was zero, most of the tracks vanished in the PN and NP experiments (Fig. 10). In contrast, if the transient eddy component from the bottom boundary was zero, the tracks decreased slightly compared with the standard experiments (Fig. 8 and 11). These sensitivity tests highlight the importance of the upstream eddies to the cyclone routes around Japan.

---

[2] This kind of experiment could, suffer from the inconsistencies between disturbances from the upstream and those generated at the surface inside the RAM.

5. Conclusion and Discussion

We have investigated the factors that control cyclone passage routes around Japan during the winter, using data analysis and RAM experiments. Data analysis revealed that the interannual variability of the cyclone routes was not related to the seasonal hemispheric flow in the troposphere with a small signal upstream of the focusing area. The RAM experiments, in which the BC was a combination of the monthly mean field for one year and the transient eddy field for another year, showed that the cyclone passage routes were highly sensitive to the transient eddies travelling from the western boundary of the calculated domain but less sensitive to the mean flow field. Both data analysis and RAM experiments suggested that the cyclone passage route around Japan was largely independent of the mean flow. Additional analysis showed that the mean flow field played an important role in the growth rate of cyclones around Japan, consistent with linear baroclinic instability theory.

Ensemble forecasting uses different initial conditions and predicts probable forecasts with its forecasting spreads by summing up the different members. Ensemble experimental techniques can be applied to hindcast experiments, where the effect of various BCs can be investigated. Similarly, the new method for boundary ensemble experiments proposed in this paper can be categorized as an ensemble experiment. However, the fabricated BCs as ensemble members are useful because the atmosphere in the RAM depends on the BCs; changing the initial conditions in the RAM for ensemble experiments was not effective. Our method therefore enables us to perform semi-realistic experiments and hindcast experiments. Mesoscale meteorology has revealed the detailed

structure of cold and warm fronts and then successfully simulated them. Using boundary ensemble simulations may allow the climatological characteristics of cold and warm fronts to be recreated. Also, the growth rate of baroclinic eddies is likely to be influenced by the sharp ocean front in the Kuroshio current and its extension (Xie et al. 2002). Minobe et al. (2008; 2010) and Taguchi et al. (2009) have recently discovered a close relationship between eddy activity and ocean fronts. Woollings et al. (2010) argued that the temporal resolution of prescribed sea surface temperatures is important. Ensemble experiments could be performed with different sea surface temperature distributions as a surface BC for the RAM. The experiments would reveal the impact of the sea surface temperature on the growth rate of eddies above. This study is potentially a milestone in extending mesoscale meteorology to a climatological description of atmospheric and ocean phenomena on a horizontal scale of tens of kilometers.

Although we focus on the boundary ensemble experiments in this paper, there are problems in the practical application of this approach. Because there is no separation of time mean field and transient eddy components in the atmosphere, a transient eddy under one mean flow state can move and develop in a different manner to the same transient eddy under another state. The combination of the mean flow in a year and the transient eddy component in a different year is therefore not entirely realistic. Even if the RAM estimate had no bias for the atmospheric simulation in the nesting area, it is possible that using the fabricated BCs with RAMs that use data from a different year, the RAM climate could be unrealistic. It would therefore be interesting to run the boundary ensemble simulations with different RAM systems, such as spectral nudging

(Kanamaru and Kanamitsu 2007; Kida et al. 1991) or anomalous nesting (Misra and Kanamitsu 2004) in order to test the new idea proposed in this paper.

Acknowledgments: We thank Prof. Shoshiro Minobe for giving us insightful comments on our earlier results. The first author is supported by a Grant-in-Aid for Young Scientists (B) 18740293, by a Grant-in-Aid for Scientific Research on Innovative Areas 22106008, by a Grant-in-Aid for Scientific Research (A) 22244057, and by Research Program on Climate Change Adaptation, all of Ministry of Education, Sports, Culture, Science, and Technology, Japan; and supported by Global Environment Research Fund S-5-3 of the Ministry of the Environment, Japan. The model simulations were performed using the Hokkaido University High Performance Computing System. All figures were drawn using Grid Application Development Software (GrADS).

References

Adachi, S., and F. Kimura, 2007: A 36-year climatology of surface cyclogenesis in East Asia under high-resolution reanalysis data. *SOLA*, **3,** 113-116.

Blackmon, M. L., 1976: A climatological spectral study of the 500 mb geopotential height of the Northern Hemisphere. *J. Atmos. Sci.*, **33,** 1607-1623.

Charney, J. G., 1947: The dynamics of long waves in a baroclinic westerly current. *J. Meteorology*, **4,** 135-162.

Eady, E., 1949: Long waves and cyclone waves. *Tellus*, **1,** 33-52.

Hoskins, B. J., and K. I. Hodges, 2002: New perspectives on the Northern Hemisphere winter storm tracks. *J. Atmos. Sci.*, **59,** 1041-1061.

Hoskins, B. J., and K. I. Hodges, 2005: New perspectives on the Southern Hemisphere winter storm tracks. *J. Climate*, **18,** 4108-4129.

Hoskins, B. J., I. N. James, and G. H. White, 1983: The shape, propagation and mean-flow interaction of large-scale weather systems. *J. Atmos. Sci.*, **40,** 1595-1612.

Inatsu, M., 2009: The neighbor enclosed area tracking algorithm for extratropical wintertime cyclones. *Atmos. Sci. Lett.*, **10,** 267-272.

Inatsu, M., and M. Kimoto, 2005: Two types of the interannual variability of the mid-winter storm-track and their relationship to the global warming. *SOLA*, **1,** 61-64.

Inatsu, M., H. Mukougawa, and S.-P. Xie, 2003: Atmospheric response to zonal variations in midlatitude SST: Transient and stationary eddies and their feedback. *J. Climate*, **16,** 3314-3329.

James, I. N., 1987: Suppression of barotropic instability in horizontally sheared flows. *J. Atmos. Sci.*, **44,** 3710-3720.

Kain, J., and J. Fritsch, 1993: Convective parameterization for mesoscale models: The Kain-Fritsch scheme. The representation of cumulus convection in numerical models. Amer. Meteor. Soc, No. 46 in Meteor. Monogr., 165-170 pp.

Kanamaru, H., and M. Kanamitsu, 2007: Scale-selective bias correction in a downscaling of global analysis using a regional model. *Mon. Wea. Rev.*, **135,** 334-350.

Kida, H., T. Koide, H. Sasaki, and M.Chiba, 1991: A new approach for coupling a limited area model to a GCM for regional climate simulations. *J. Meteor. Soc. Japan*, **69,** 723-728.

Kusaka, H., and H. Kitahata, 2009: Synoptic-scale climatology of cold frontal precipitation systems during the passage over central Japan. *SOLA*, **5,** 61-64

Minobe, S., A. Kuwano-Yoshida, N. Komori, S. P. Xie, and R. J. Small, 2008: Influence of the Gulf Stream on the troposphere. *Nature*, **452,** 206-209.

Minobe, S., M. Miyashita, A. Kuwano-Yoshida, H. Tokinaga, and S.-P. Xie, 2010: Atmospheric response to the Gulf Stream: Seasonal variations. *J. Climate*, **23,** 3699-3719.

Misra, V., and M. Kanamitsu, 2004: Anomaly nesting: A methodology to downscale seasonal climate simulations from AGCMs. *J. Climate*, **17,** 3249-3262.

Murray, R. J., and I. Simmonds, 1991: A numerical scheme for tracking cyclone centers from digital data. Part I: Development and operation of the scheme. *Aust. Meteor. Mag.*, **39,** 155-166.

Nakamura, H., 1992: Midwinter suppression of baroclinic wave activity in the Pacific. *J. Atmos. Sci.*, **49,** 1629-1642.

Nakamura, H., T. Izumi, and T. Sampe, 2002: Interannual and decadal modulations recently observed in the Pacific storm track activity and East Asian winter monsoon. *J. Climate*, **15,** 1855-1874.

Nakamura, H., T. Sampe, Y. Tanimoto, and A. Shimpo, 2004: Observed associations among storm tracks, jet streams and mid-latitude oceanic fronts. *Ocean-atmosphere interaction and climate variability*, Geophys. Monogr., Amer. Geophys. Union, 329-346.

Nishii, K., T. Miyasaka, Y. Kosaka, and H. Nakamura, 2009: Reproducibility and future projection of the midwinter storm-track activity over the Far East in the CMIP3 climate models in relation to "Haru-Ichiban" over Japan. *J. Meteor. Soc. Japan*, **81,** 581-587.

Onogi, K., and Coauthors, 2007: The JRA-25 reanalysis. *J. Meteor. Soc. Japan*, **85,** 369-432.

Saito, K., and Coauthors, 2006: The operational JMA nonhydrostatic mesoscale model. *Mon. Wea. Rev.*, **134,** 1266-1298.

Sanders, F., and J. R. Gyakum, 1980: Synoptic-dynamic climatology of the "bomb". *Mon. Wea. Rev.*, **108,** 1589-1606.

Sinclair, M. R., 1994: An objective cyclone climatology for the Southern Hemisphere. *Mon. Wea. Rev.*, **122,** 2239-2256.

Taguchi, B., H. Nakamura, M. Nonaka, and S.-P. Xie, 2009: Influences of the Kuroshio/Oyashio Extensions on air-sea heat exchanges and storm-track activity as revealed in regional atmospheric model simulations for the 2003/4 cold season. *J. Climate*, **22,** 6536-6560.

Takano, I., 2002: Analysis of an intense winter extra-tropical cyclone that advanced along the South coast of Japan. *J. Meteor. Soc. Japan*, **80,** 669-685.

Takayabu, I., 1991: "Coupling Development": An Efficient Mechanism for the Development of Extratropical Cyclones. *J. Meteor. Soc. Japan*, **69,** 609-621.

Thorncroft, C. D., B. J. Hoskins, and M. E. McIntyre, 1993: Two paradigms of baroclinic-wave life-cycle behaviour. *Quart. J. Roy. Meteor. Soc.*, **119,** 17-55.

Trenberth, K. E., 1991: Storm tracks in the Southern Hemisphere. *J. Atmos. Sci.*, **48,** 2159-2178.

Wallace, J. M., G.-H. Lim, and M. L. Blackmon, 1988: Relationship between cyclone tracks, anticyclone tracks and baroclinic waveguides. *J. Atmos. Sci.*, **45,** 439-462.

Woollings, T., B. Hoskins, M. Blackburn, D. Hassell, and K. Hodges, 2010: Storm track sensitivity to sea surface temperature resolution in a regional atmosphere model. *Climate Dynamics*, **35,** 341-353.

Xie, S.-P., J. Hanfer, Y. Tanimoto, W. Liu, H. Tokinaga, and H. Xu, 2002: Bathymetric effect on the winter sea surface temperature and climate of the

Yellow and East China Seas. *Geophys. Res. Lett.*, **29,** doi:10.1029/2002GL015884.

Yin, J. H., 2005: A consistent poleward shift of the storm tracks in simulations of 21st century climate. *Geophysical Research Letters*, **32,** doi 10.1029/2005gl023684.

Yoshida, A., and Y. Asuma, 2004: Structures and environment of explosively developing extra-tropical cyclones in the Northwestern Pacific region. *Mon. Wea. Rev.*, **132,** 1121-1142.

Yoshiike, S., and R. Kawamura, 2009: Influence of wintertime large-scale circulation on the explosively developing cyclones over the western North Pacific and their downstream effects. *J. Geophys. Res.*, **114,** D13110, doi:13110.11029/12009JD011820.

List of Table and Figures

Table 1: Experiment nomenclature. Columns and rows in the table denote a selective December January February (DJF) for the 30 day mean and transient components of the boundary conditions (BCs), respectively. The experiment name consists of the combination of the mean and transient components of the BC as prefix and suffix, respectively. The letters P, p, N, and n indicate DJFs from 2007/08, 1983/84, 1989/90, and 1987/88, respectively.

Figure 1: (a) DJF climatology of track density based on Vh850 with a contour interval of 1 (average track length)$^{-1}$ (3 month)$^{-1}$, thick lines every 2 (average track length)$^{-1}$ (3 month)$^{-1}$, and shaded areas for values > 8 (average track length)$^{-1}$ (3 month)$^{-1}$. (b) DJF climatology of the high-pass filtered meridional wind variance at 850 hPa (Vh850). The contour interval is 5 m^2 s^{-2} with thick lines every 10 m^2 s^{-2} and shaded areas for values > 20 m^2 s^{-2}.

Figure 2: Interannual variability of cyclone density in DJF. (a) The first mode of the empirical orthogonal function (EOF) for track density based on Vh850. The contour interval is 0.5 L^{-1} (3 month)$^{-1}$, with > 95% statistically significant areas shaded. (b) First Principal Component (PC) of Vh850 track density. The linear trend of the first mode of track density variability is 0.02 yr^{-1}.

Figure 3: Composite of track density based on Vh850 in DJF. (a) The composite for positive years on the first EOF mode of 2007/08, 1983/84, 2002/03, and 1994/95, and (b) the composite for negative years of 1989/90, 1987/88, 1986/87,

and 1984/85. The contour interval is 0.5 L^{-1} (3 month)$^{-1}$, with > 95% statistically significant areas shaded.

Figure 4: Composite maps of (contour) 500 hPa geopotential height and (shading) 300 hPa zonal wind for (a) positive Nangan cyclone DJFs and (b) for negative Nangan cyclone DJFs. The contour interval is 60 m. (c) Regression of 500 hPa geopotential height on the first mode of the cyclone track density. The contour interval is 5 m with thick lines every 10 m. Shading denotes a statistical significance above 95%. (d) Regression of 300 hPa zonal wind on the first mode of the cyclone track density. The contour interval is 1 m s^{-1} with thick lines every 2 m s^{-1}. Shading denotes a statistical significance above 95%.

Figure 5: The track density based on Vh850 in DJF for the ensemble means of the regional model experiments; (a) P*-ensemble, (b) N*-ensemble, (c) *P-ensemble, and (d) *N-ensemble. The contour interval is 1 L^{-1} (month)$^{-1}$ and the shading denotes values above > 4 L^{-1} (month)$^{-1}$.

Figure 6: The track density based on Vh850 in DJF for the ensemble means of the regional model experiments; (a) PP-ensemble, (b) PN-ensemble, (c) NP-ensemble, and (d) NN-ensemble. The contour interval is 1 L^{-1} (month)$^{-1}$ and the shading denotes values above > 4 L^{-1} (month) $^{-1}$.

Figure 7: The track density based on Vh850 in DJF for the ensemble means of the regional model experiments; (a) PP-ensemble, (b) PN-ensemble, (c) NP-

ensemble, and (d) NN-ensemble. The average growth rate (unit is day^{-1}) has contours of 0.1, 0.2, 0.33, 0.5, 0.67, 1, 1.5, 2, 3, 5, and 10 day^{-1}.

Figure 8: The track density based on Vh850 in DJF for the ensemble means of the regional model experiments; (a) PN and (b) NP, which are used as reference experiments. The contour interval is 1 L^{-1} $(month)^{-1}$ and the shading denotes values above > 4 L^{-1} $(month)^{-1}$.

Figure 9: The track density based on Vh850 in DJF for the ensemble means of the regional model experiments; (a) PN and (b) NP, where the mean flow and eddy components are regarded as fluctuations with a period of more than and less than 10 days, respectively The contour interval is 1 L^{-1} $(month)^{-1}$ and the shading denotes values above > 4 L^{-1} $(month)^{-1}$.

Figure 10: The track density based on Vh850 in DJF for the ensemble means of the regional model experiments; (a) PN and (b) NP, where the eddy component of western lateral BC is set to zero. The contour interval is 1 L^{-1} $(month)^{-1}$ and the shading denotes values above > 4 L^{-1} $(month)^{-1}$.

Figure 11: The track density based on Vh850 in DJF for the ensemble means of the regional model experiments; (a) PN and (b) NP, where the eddy component of bottom BC is set to zero. The contour interval is 1 L^{-1} $(month)^{-1}$ and the shading denotes values above > 4 L^{-1} $(month)^{-1}$.

Table 1: Experiment nomenclature. Columns and rows in the table denote a selective December January February (DJF) for the 30 day mean and transient components of the boundary conditions (BCs), respectively. The experiment name consists of the combination of the mean and transient components of the BC as prefix and suffix, respectively. The letters P, p, N, and n indicate DJFs from 2007/08, 1983/84, 1989/90, and 1987/88, respectively.

mean/ transient	07/08	89/90	83/84	87/88
07/08	PP	Pp	PN	Pn
89/90	pP		pN	
83/84	NP	Np	NN	Nn
87/88	nP		nN	

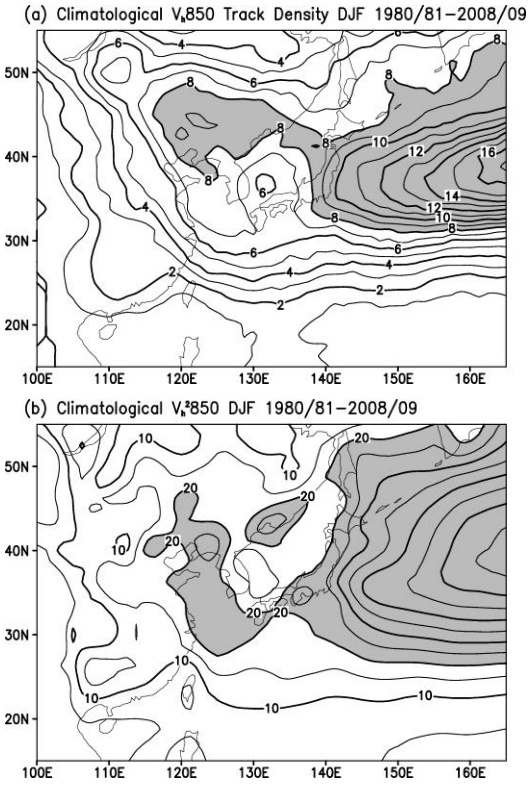

Figure 1: (a) DJF climatology of track density based on Vh850 with a contour interval of 1 (average track length)$^{-1}$ (3 month)$^{-1}$, thick lines every 2 (average track length)$^{-1}$ (3 month)$^{-1}$, and shaded areas for values > 8 (average track length)$^{-1}$ (3 month)$^{-1}$. (b) DJF climatology of the high-pass filtered meridional wind variance at 850 hPa (Vh850). The contour interval is 5 m^2 s^{-2} with thick lines every 10 m^2 s^{-2} and shaded areas for values > 20 m^2 s^{-2}.

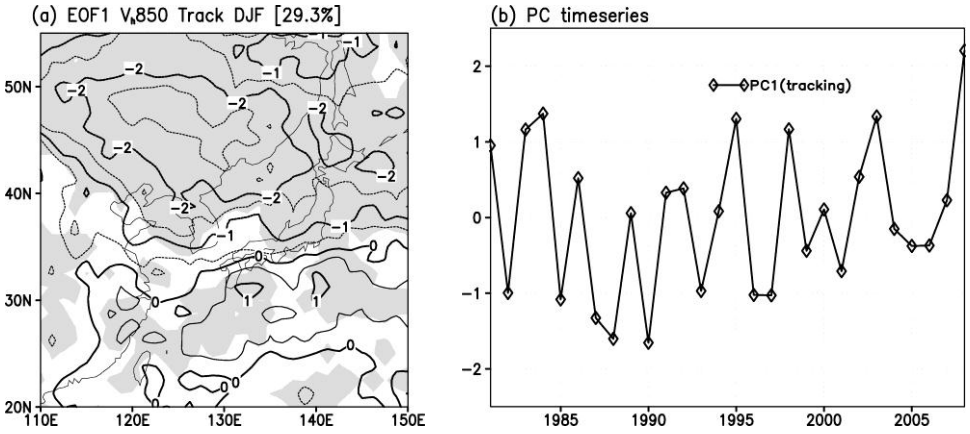

Figure 2: Interannual variability of cyclone density in DJF. (a) The first mode of the empirical orthogonal function (EOF) for track density based on Vh850. The contour interval is 0.5 L^{-1} $(3\ month)^{-1}$, with > 95% statistically significant areas shaded. (b) First Principal Component (PC) of Vh850 track density. The linear trend of the first mode of track density variability is 0.02 yr^{-1}.

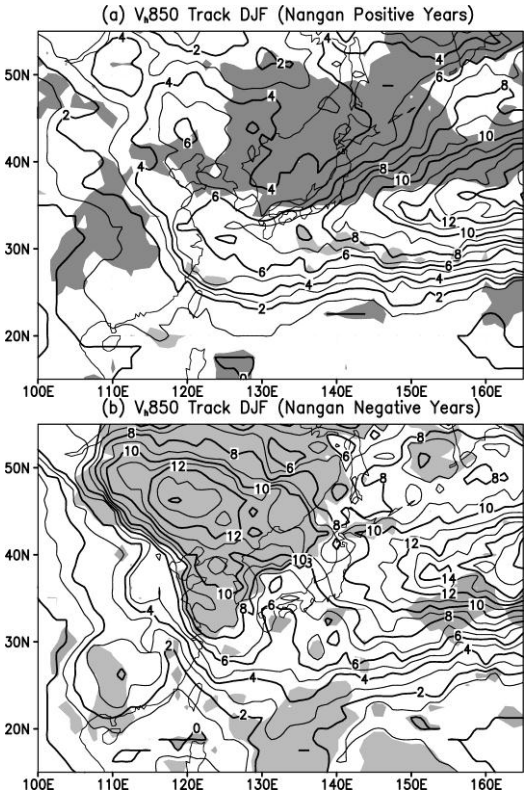

Figure 3: Composite of track density based on Vh850 in DJF. (a) The composite for positive years on the first EOF mode of 2007/08, 1983/84, 2002/03, and 1994/95, and (b) the composite for negative years of 1989/90, 1987/88, 1986/87, and 1984/85. The contour interval is 0.5 L^{-1} $(3\ month)^{-1}$, with > 95% statistically significant areas shaded.

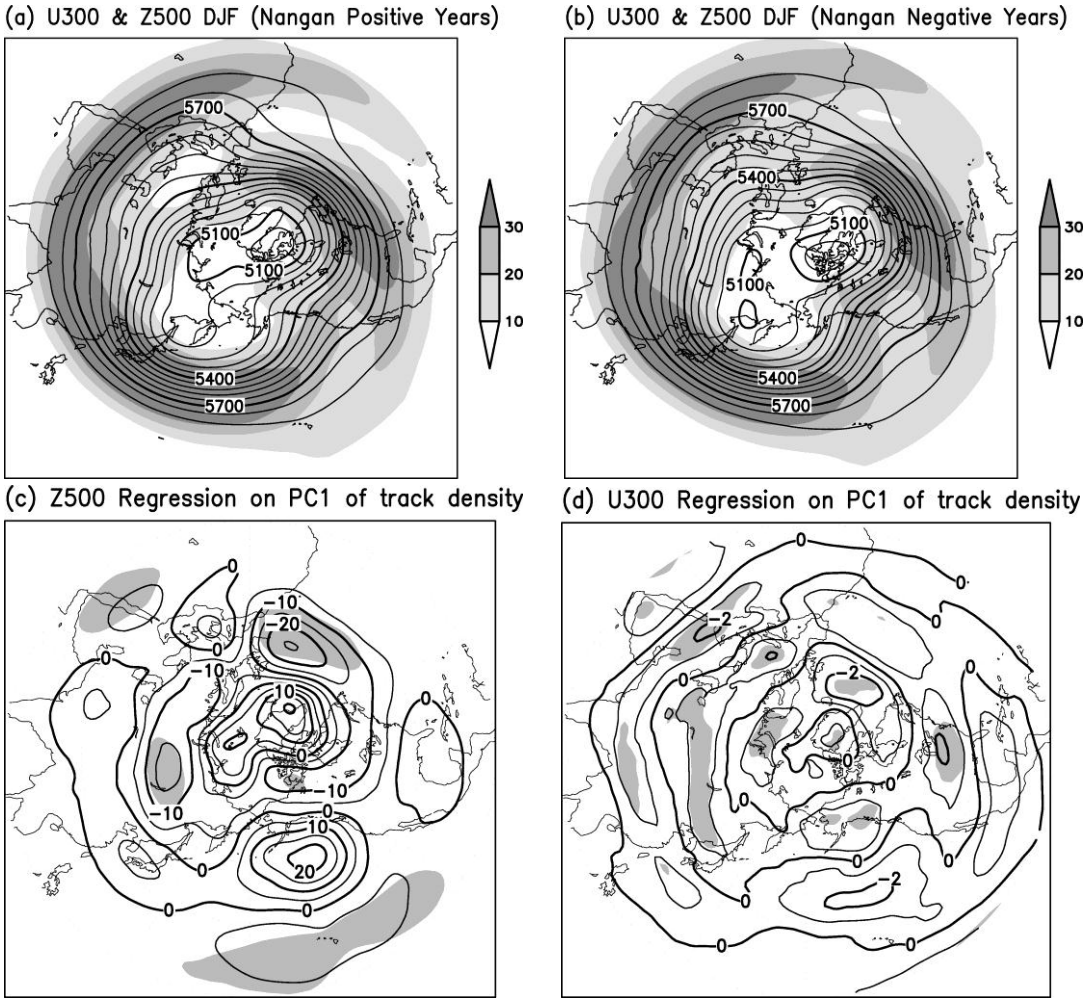

Figure 4: Composite maps of (contour) 500 hPa geopotential height and (shading) 300 hPa zonal wind for (a) positive Nangan cyclone DJFs and (b) for negative Nangan cyclone DJFs. The contour interval is 60 m. (c) Regression of 500 hPa geopotential height on the first mode of the cyclone track density. The contour interval is 5 m with thick lines every 10 m. Shading denotes a statistical significance above 95%. (d) Regression of 300 hPa zonal wind on the first mode of the cyclone track density. The contour interval is 1 m s^{-1} with thick lines every 2 m s^{-1}. Shading denotes a statistical significance above 95%.

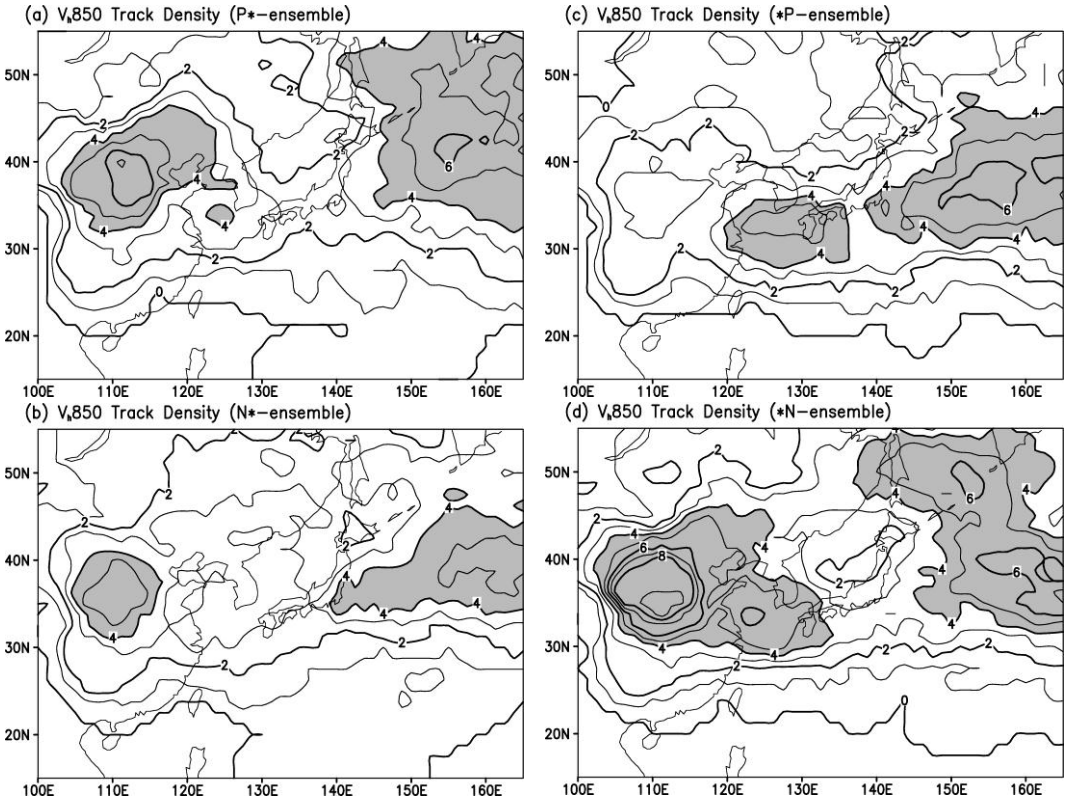

Figure 5: The track density based on Vh850 in DJF for the ensemble means of the regional model experiments; (a) P*-ensemble, (b) N*-ensemble, (c) *P-ensemble, and (d) *N-ensemble. The contour interval is 1 L^{-1} $(month)^{-1}$ and the shading denotes values above > 4 L^{-1} $(month)^{-1}$.

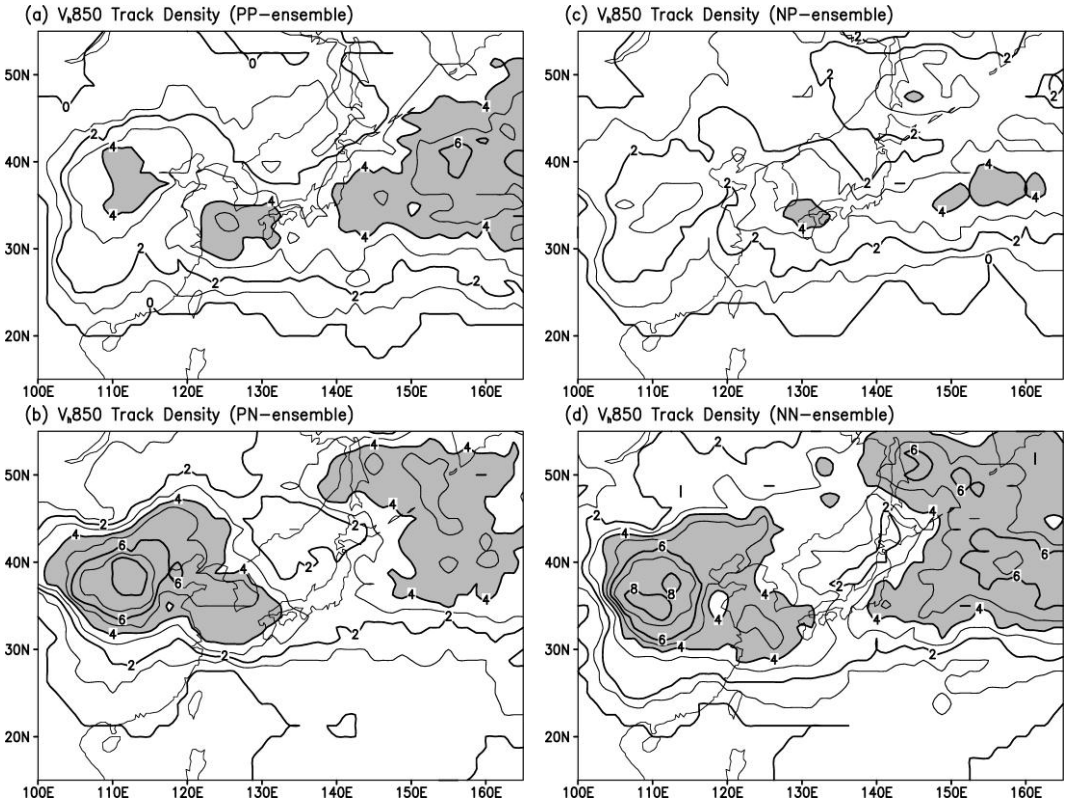

Figure 6: The track density based on Vh850 in DJF for the ensemble means of the regional model experiments; (a) PP-ensemble, (b) PN-ensemble, (c) NP-ensemble, and (d) NN-ensemble. The contour interval is 1 L^{-1} $(month)^{-1}$ and the shading denotes values above > 4 L^{-1} $(month)^{-1}$.

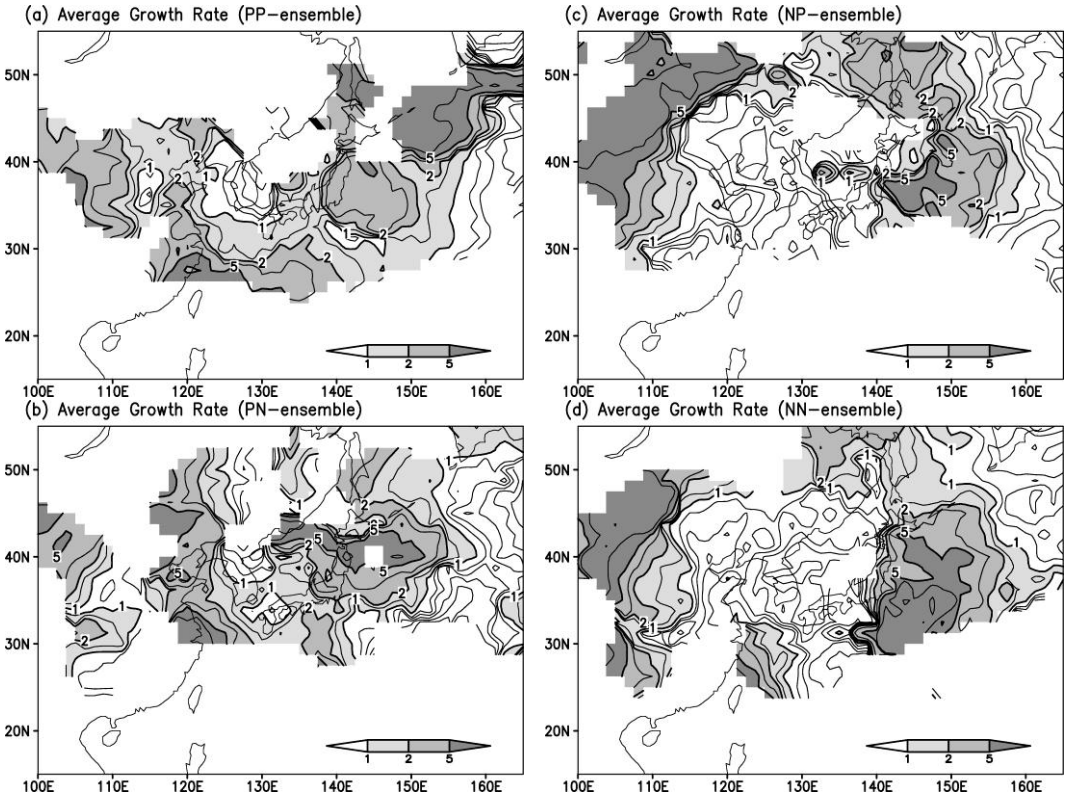

Figure 7: The track density based on Vh850 in DJF for the ensemble means of the regional model experiments; (a) PP-ensemble, (b) PN-ensemble, (c) NP-ensemble, and (d) NN-ensemble. The average growth rate (unit is day^{-1}) has contours of 0.1, 0.2, 0.33, 0.5, 0.67, 1, 1.5, 2, 3, 5, and 10 day^{-1}.

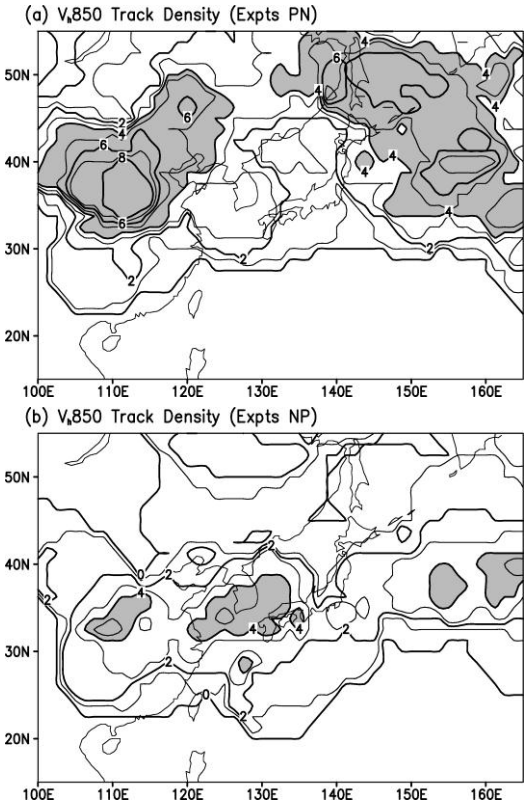

Figure 8: The track density based on Vh850 in DJF for the ensemble means of the regional model experiments; (a) PN and (b) NP, which are used as reference experiments. The contour interval is 1 L^{-1} $(month)^{-1}$ and the shading denotes values above > 4 L^{-1} $(month)^{-1}$.

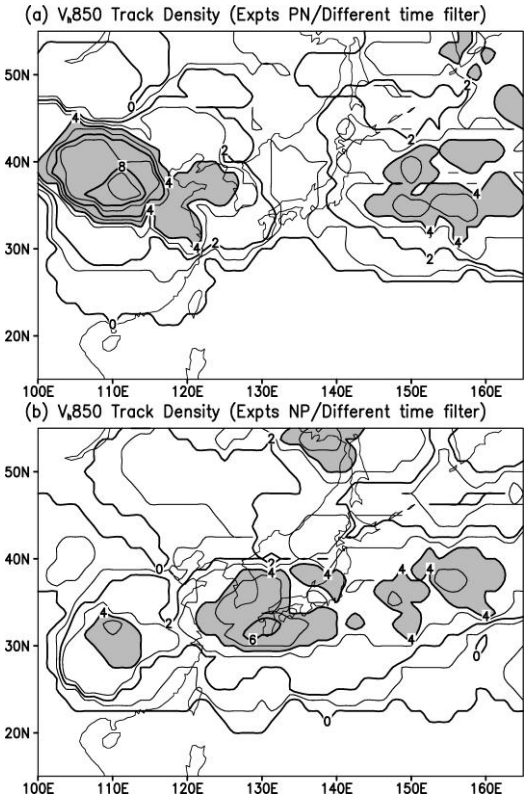

Figure 9: The track density based on Vh850 in DJF for the ensemble means of the regional model experiments; (a) PN and (b) NP, where the mean flow and eddy components are regarded as fluctuations with a period of more than and less than 10 days, respectively The contour interval is 1 L^{-1} $(month)^{-1}$ and the shading denotes values above > 4 L^{-1} $(month)^{-1}$.

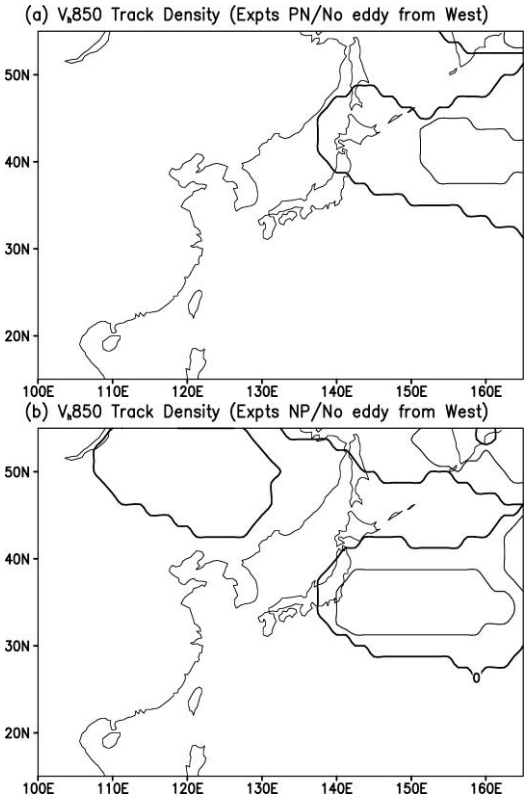

Figure 10: The track density based on Vh850 in DJF for the ensemble means of the regional model experiments; (a) PN and (b) NP, where the eddy component of western lateral BC is set to zero. The contour interval is 1 L^{-1} $(month)^{-1}$ and the shading denotes values above > 4 L^{-1} $(month)^{-1}$.

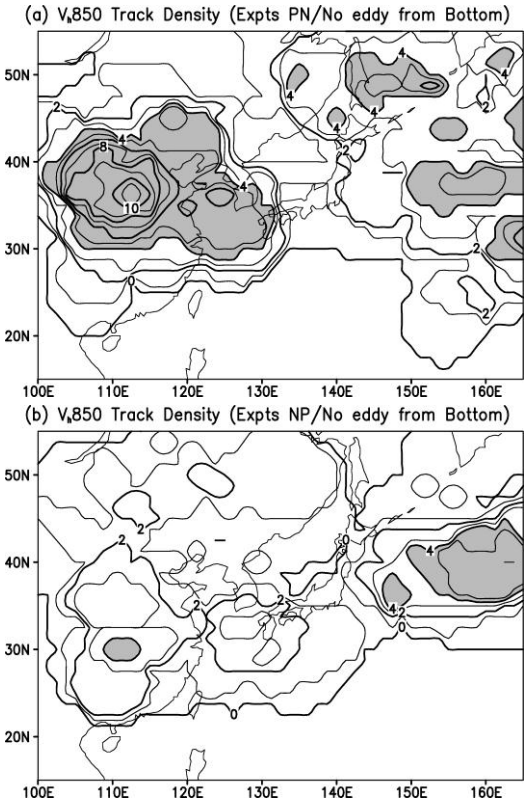

Figure 11: The track density based on Vh850 in DJF for the ensemble means of the regional model experiments; (a) PN and (b) NP, where the eddy component of bottom BC is set to zero. The contour interval is 1 L^{-1} $(month)^{-1}$ and the shading denotes values above > 4 L^{-1} $(month)^{-1}$.